nanomaterials

MDPI

Article

Thermoelectric Characteristics of A Single-Crystalline Topological Insulator Bi_2Se_3 Nanowire

Dedi [1,2,*], Ping-Chung Lee [2], Pai-Chun Wei [3] and Yang-Yuan Chen [2]

[1] Research Center for Electronics and Telecommunications (P2ET), Indonesian Institute of Sciences (LIPI), Bandung 40135, Indonesia
[2] Institute of Physics, Academia Sinica, Taipei 11529, Taiwan; plexlee@gmail.com (P.-C.L.); cheny2@phys.sinica.edu.tw (Y.-Y.C.)
[3] Center for Condensed Matter Sciences and Center of Atomic Initiatives for New Materials, National Taiwan University, Taipei 10617, Taiwan; pcwei68@gmail.com
* Correspondence: dedi030@lipi.go.id; Tel.: +62-22-250-4660

Abstract: The discovery of topological insulators (TIs) has motivated detailed studies on their physical properties, especially on their novel surface states via strong spin–orbit interactions. However, surface-state-related thermoelectric properties are rarely reported, likely because of the involvement of their bulk-dominating contribution. In this work, we report thermoelectric studies on a TI bismuth selenide (Bi_2Se_3) nanowire (NW) that exhibit a larger surface/volume ratio. Uniform single-crystalline TI Bi_2Se_3 NWs were successfully synthesized using a stress-induced growth method. To achieve the study of the thermoelectric properties of a nanowire (NW), including electrical conductivity (σ), Seebeck coefficient (S), and thermal conductivity (κ), a special platform for simultaneously performing all measurements on a single wire was designed. The properties of σ, S, and κ of a 200 nm NW that was well precharacterized using transmission electron microscope (TEM) measurements were determined using the four-probe method, the two-probe EMF across ∇T measurement, and the 3ω technique, respectively. The integrated TE properties represented by the figure of merit ZT ($S^2\sigma T/\kappa$) were found to be in good agreement with a theoretical study of Bi_2Se_3 NW.

Keywords: thermoelectric; bismuth selenide; nanowire

Citation: Dedi; Lee, P.-C.; Wei, P.-C.; Chen, Y.-Y. Thermoelectric Characteristics of A Single-Crystalline Topological Insulator Bi_2Se_3 Nanowire. *Nanomaterials* **2021**, *11*, 819. https://doi.org/10.3390/nano11030819

Academic Editor: Matthias Elm

Received: 21 February 2021
Accepted: 20 March 2021
Published: 23 March 2021

1. Introduction

The study of nanoengineered thermoelectric materials used for converting waste heat into electricity has become a compelling research topic [1–5]. The thermoelectric (TE) generator and the TE sensor are devices that can harvest renewable energy for power generation and thermal sensing, respectively [6–11]. The efficiency of TE materials is determined by the dimensionless figure of merit ZT, which is defined as $S^2\sigma T/(\kappa_e + \kappa_l)$, where S is the TE power or Seebeck coefficient, σ represents the electrical conductivity, κ_e is the electronic thermal conductivity, and κ_l is the lattice thermal conductivity. The quantity $S^2\sigma$ is defined as the power factor (PF). The Weidmann–Franz law restricts the ratio σ/κ in a bulk TE compound. Furthermore, a sharply peaked density of states (DOS) favors a large S, while the density of states in bulk materials is a smoothly variable function. As dimensionality is reduced from three to one, the electronic DOS at the energy-band edges is significantly increased, increasing the TE PF ($S^2\sigma$) and yielding an improved ZT [12,13]. Then, according to Dresselhaus et al., 1D nanowires can boost thermoelectric performance [13,14]. A Bi nanowire would also have a reduced κ due to phonon scattering off the sidewalls, which helps increase ZT, based on a previous study [13,15].

Slack et al. reported that semiconductors exhibiting narrow band gaps and high mobility carriers are optimal TE materials [16]. Bi_2Se_3 is a V–VI topological-insulator material that exhibits a narrow band gap of approximately 0.3 eV and crystallizes in a rhombohedral structure belonging to the tetradymite space group D^5_{3d} (R-3m) [17–19]. This

material demonstrates potential for application in optical recording systems [20], photoelectrochemical devices [21], and TE devices [17,18]. In recent years, bismuth chalcogenides have attracted substantial research interest because of their superior TE properties of high *ZT* at room temperature [22]. Diverse synthesis techniques have been developed to synthesize various nanostructures of Bi_2Se_3, such as microwave heating [23,24], a single-source precursor method [25–27], solvothermal method [28–30], the metal–organic chemical vapor deposition method [31,32], and mechanical exfoliation [33–35], whereas the commonly used synthesis method for producing Bi_2Se_3 bulk single-crystalline material is based on the Bridgman technique [36–41]. However, only a few studies have been reported on growing Bi_2Se_3 NWs and characterizing their TE properties.

2. Materials and Methods

We previously synthesized PbTe NWs from a PbTe thin film (TF) on a SiO_2/Si substrate using a stress-induced method [42,43] based on a mechanism in which mismatched thermal expansion between a substrate and deposited film drove the mass flow along grain boundaries at thermal annealing temperatures. This innovative NW-growth method (which does not involve conventional templates, catalysts, or starting materials) enables us to control growth conditions for growing different diameters, shapes, and aspect ratios of single-crystalline NWs [44,45], thus enabling exploration of any possible novel TE property of Bi_2Se_3 NWs.

The starting Bi_2Se_3 crystalline ingot was synthesized from Bi and Se source materials using the Bridgman method. Bi (99.999%, −200 mesh, Alfa Aesar, Lancashire, UK) and Se (99.999%, −200 mesh, Alfa Aesar, Lancashire, UK) powders were first mixed at a 2:3 ratio and then melted at 800 °C for 4 h in a vacuumed quartz tube at a pressure less than 5×10^{-6} torr. The molten compound was slowly cooled in the furnace to room temperature. Subsequently, a pellet specimen cut from the compound served as the target for pulsed laser deposition (PLD). Single-crystal SiO_2/Si (100) wafers (E-light Tech. Inc. Taipei, Taiwan; SiO_2 thickness = 1μm; diameter = 100 ± 0.5 mm) with double-side polishing were cut into 1.5 × 1.5 cm^2 squares for substrates. All substrates were cleaned using acetone, isopropyl alcohol, and deionized water in an ultrasonic bath for 10 min before being dried with an N_2 stream. The Bi_2Se_3 films were fabricated using an ArF excimer laser (Lambda Physik LPXPro 210, Santa Clara, California, USA) and deposited onto substrates in a vacuum system with a base pressure of 5.0×10^{-7} torr. The Bi_2Se_3 TFs were grown at a deposition rate of 0.3 Å/s, and the excimer laser was applied at 140 mJ (frequency = 10 Hz) for 15 min at room temperature. The substrate was rotated at approximately 10 rpm, and the film thickness was 30 nm. The films were sealed in a vacuumed quartz tube at less than 5×10^{-6} torr for annealing at 450 °C for 5 d, followed by cooling the furnace to room temperature. During the annealing process, Bi_2Se_3 NWs grew from the film via the different thermal expansion coefficients of the Bi_2Se_3 film (19×10^{-6}/°C) [46] and the SiO_2/Si substrate (0.5×10^{-6}/°C)/(2.4×10^{-6}/°C) [42–45].

3. Results and Discussion

3.1. Characterization of Materials

Field emission scanning electron microscopy (Hitachi Co., S-4800, Tokyo, Japan) images of the Bi_2Se_3 NWs (Figure 1a) showed that the NWs exhibited diameters ranging from 50 to 500 nm and lengths up to 100 μm. Straight and uniform Bi_2Se_3 NWs of high aspect ratio grew on the substrate after annealing. A tungsten needle (*d* = 100 nm) and a binocular optical microscope were used to extract a single-crystal NW from the Bi_2Se_3 film; the NW was then suspended on a Si_3N_4 microchip by using electrodes (Figure 1b) and employed in structural analyses and thermoelectricity measurements. A transmission electron microscope (TEM; JEOL JEM-2100 at 200 kV, Tokyo, Japan) was used to examine the crystalline structure of the Bi_2Se_3 NW (Figure 1c,d).

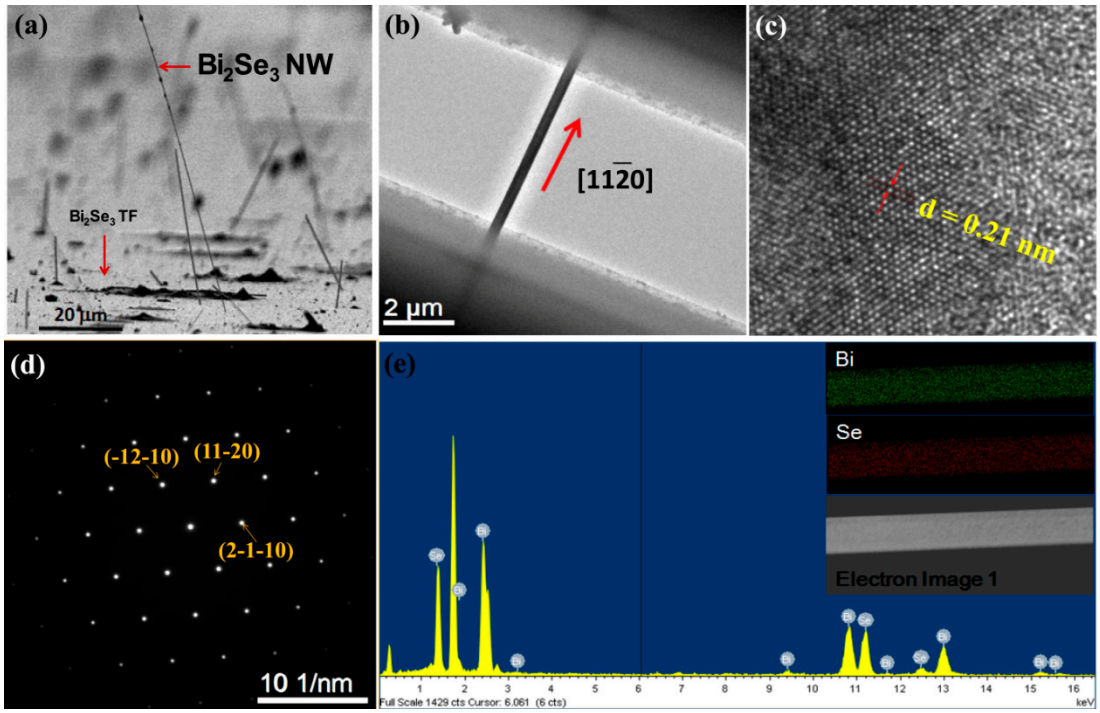

Figure 1. (**a**) SEM image (top view) indicating that all Bi_2Se_3 NWs grew several micrometers in length from the surface of the Bi_2Se_3 TF; (**b**) TEM images of a single-crystal Bi_2Se_3 NW suspended on a Si_3N_4 microchip following electrode formation by using a FIB that served as the TEM holder; (**c**) HR-TEM image of the NW shown in (**b**), where the distance between crystal faces is 0.21 nm; (**d**) the SAED pattern (at the [0001] zone axis), confirming that the single-crystalline NWs grew in the [11–20] direction; and (**e**) EDS spectrum of a Bi_2Se_3 NW (the inset shows the EDS mapping image of a NW).

The electrical resistivity ρ and Seebeck coefficient S of the Bi_2Se_3 bulk were measured simultaneously using commercial equipment (ZEM-3, ULVAC-RIKO, Chigasaki, Kanagawa, Japan) in a He atmosphere from 300 to 540 K. The thermal conductivity κ of the Bi_2Se_3 bulk was calculated using the equation $\kappa = D.C_p.d$, where D is the thermal diffusivity, C_p is the specific heat, and d is the density of the sample. The thermal diffusivity D was examined via a laser-flash apparatus (NETZSCH, LFA 457, Selb, Germany), and the density d was obtained using the Archimedes method (presented in Figure S1, electronic supporting information (ESI)). The Seebeck coefficient S and the electrical resistivity ρ of an NW were measured using a conventional steady-state method in an Oxford cryostat. The NW thermal conductivity was measured using the 3ω method.

The TEM image (TEM; JEOL JEM-2100 at 200 kV, Tokyo, Japan) in Figure 1c reveals that the ordered hexagonal structure exhibiting lattice fringes of 0.21 nm gaps between the [11–20] planes were consistent with those of other lattice spacing measurements of Bi_2Se_3 NWs [47]. A corresponding selected area electron diffraction (SAED) pattern (Figure 1d) reveals that the Bi_2Se_3 NWs were high-quality single crystals that exhibited growth along the [11–20] direction. The chemical composition of the Bi_2Se_3 NW was examined using energy dispersive X-ray spectroscopy (EDS, JEOL, Tokyo, Japan); the EDS mapping shown in the inset of Figure 1e indicates the uniform spatial distribution of Bi and Se elements throughout the NW.

Figure 2 presents SEM images of a Bi_2Se_3 NW (d = 200 nm) suspended on a Si_3N_4 microchip with a Pt/C electrical contact between the Bi_2Se_3 NW and the 10 nm Ni/50 nm Au electrodes deposited by a focus ion beam (FIB). The sample used in this study showed nearly an ohmic contact. Subsequently, the microchip was used to determine the values of electrical resistivity ρ and S via four-point measurements.

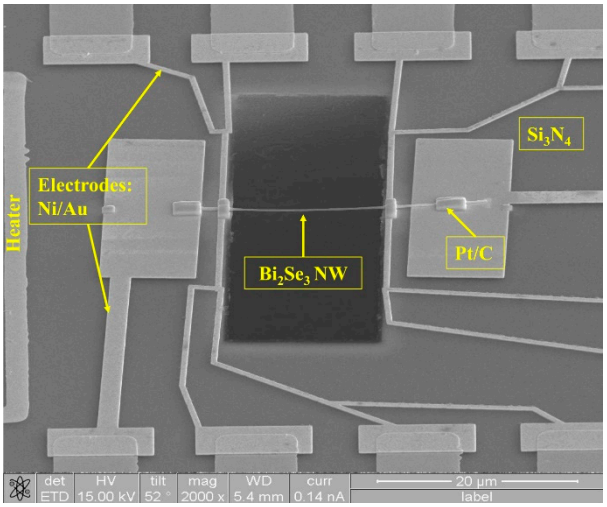

Figure 2. SEM images of a single-crystal Bi_2Se_3 NW (diameter = 200 nm) placed on a Si_3N_4 microchip following electrode formation by using a FIB.

3.2. Characterization of Thermoelectric Properties

Figure 3a shows the temperature dependence of the electrical resistance at 290–320 K for a 200 nm Bi_2Se_3 NW that exhibited weak metallic conductivities. The σ of the NW at near room temperature was 150,767 $\times$ 10^5 S m^{-1}, which was approximately 55% lower than that of the Bi_2Se_3 bulk single-crystal (27,550 $\times$ 10^5 S m^{-1}) [41] (Figure 3b). Furthermore, the surface scattering of charge carriers typically yields a reduced σ value [48]. However, the σ values of the Bi_2Se_3 NW at room temperature was higher than those reported in previous studies on the Bi_2Se_3 bulk [23–26,28,29,32], and even higher than that of the Bi_2Se_3 single-crystal made by Hor et al. [39], probably the result of the increased contribution of conduction surfaces up to 73% of the total electrical conduction upon decreasing the NW dimension via the high surface-to-volume ratio s/v ~ 2 nm^{-1} of the nanowires. A previous report [19] of electrical transport experiments on Bi_2Te_3 and Bi_2Se_2Te nanowires in the range of 200–300 nm in diameter revealed that the two-dimensional TI surface channels contribute up to 30–70% of the total electrical conduction at surface-to-volume ratios of s/v = 2−5 $\times$ 10^{-2} nm^{-1}.

The *S* values with the negative sign obtained for the Bi_2Se_3 NW (Figure 3c) show that the Bi_2Se_3 NW is an n-type semiconductor, because electrons have much higher mobility than holes and dominate the transport [49,50]. This is reasonable because undoped Bi_2Se_3 is strongly n-type [51]. Furthermore, the room temperature *S* values for the *n*-type Bi_2Se_3 NW was −51 µVK^{-1} for the 200 nm NW, the value was comparable to those typically reported by Greenaway and Harbeke for this material (i.e., in the −55 to −73 µVK^{-1} range) [52], indicating that the Fermi level lay well inside the conduction band. The magnitude of the *S* smoothly increased as the temperature increased. This behavior was consistent with that expected of a metallically doped material. The magnitude of *S* for the NW tends to be zero when the temperature is decreased because *S* represents the entropy per electric charge and must decrease to zero at 0 K [15]. Figure 3d indicates the temperature dependence of the *PF* of Bi_2Se_3 NW, indicating that the *PF* increased as temperature increased; this can be attributed to the increase in the *S* with the temperature of the Bi_2Se_3 NW. The *PF* value of the 200 nm Bi_2Se_3 NW at room temperature was 39.32 $\times$ 10^{-5} W$m^{-1}K^{-2}$, which was higher than the *PF* of the Bi_2Se_3 bulk nanostructures [21–24,26,27,31]. The enhanced *PF* value is likely a result of enhanced electronic transport of the NW.

For semiclassical transport (metals or degenerate semiconductors) the carrier-density dependence of the thermopower is described by the Mott relation [53–55]:

$$S = \frac{8\pi^2 k_B^2 T}{3qh^2} m^* \left(\frac{\pi}{3n}\right)^{\frac{2}{3}} \quad (1)$$

where k_B is Boltzmann's constant, q is the electron charge, h is Planck's constant, T is the measurement temperature, m^* is the effective mass of the carrier (m^* = 0.14 m_o in Bi_2Se_3) [56] and m_o is the electron mass. This formula is valid for assessing metals or degenerate semiconductors that exhibit an n value in the range of 10^{18} to 10^{20} cm^{-3} [57,58]. The value of n is in the range of 1.26–1.35 × 10^{19} cm^{-3} at 290–320 K for the 200 nm NW (Figure 4), indicating that the NW is a degenerate semiconductor. This value is close to that calculated by Boechko et al. for n-type single crystals of a Bi_2Se_3 single crystal (1–4 × 10^{19} cm^{-3}) [59]. The value of n increased as the temperature increased, indicating the intrinsic condition [60], with the number of thermally generated carriers exceeding the number of donor carriers. The intrinsic carrier concentration in a material n_i is generally much smaller than the dopant carrier concentration at room temperature, but n_i (=$n \cdot p$) has a very strong temperature dependence:

$$n_i \propto T^{1.5} e^{-\frac{E_{g0}}{2kT}} \quad (2)$$

where E_{g0} is the energy band gap at T = 0 K [60].

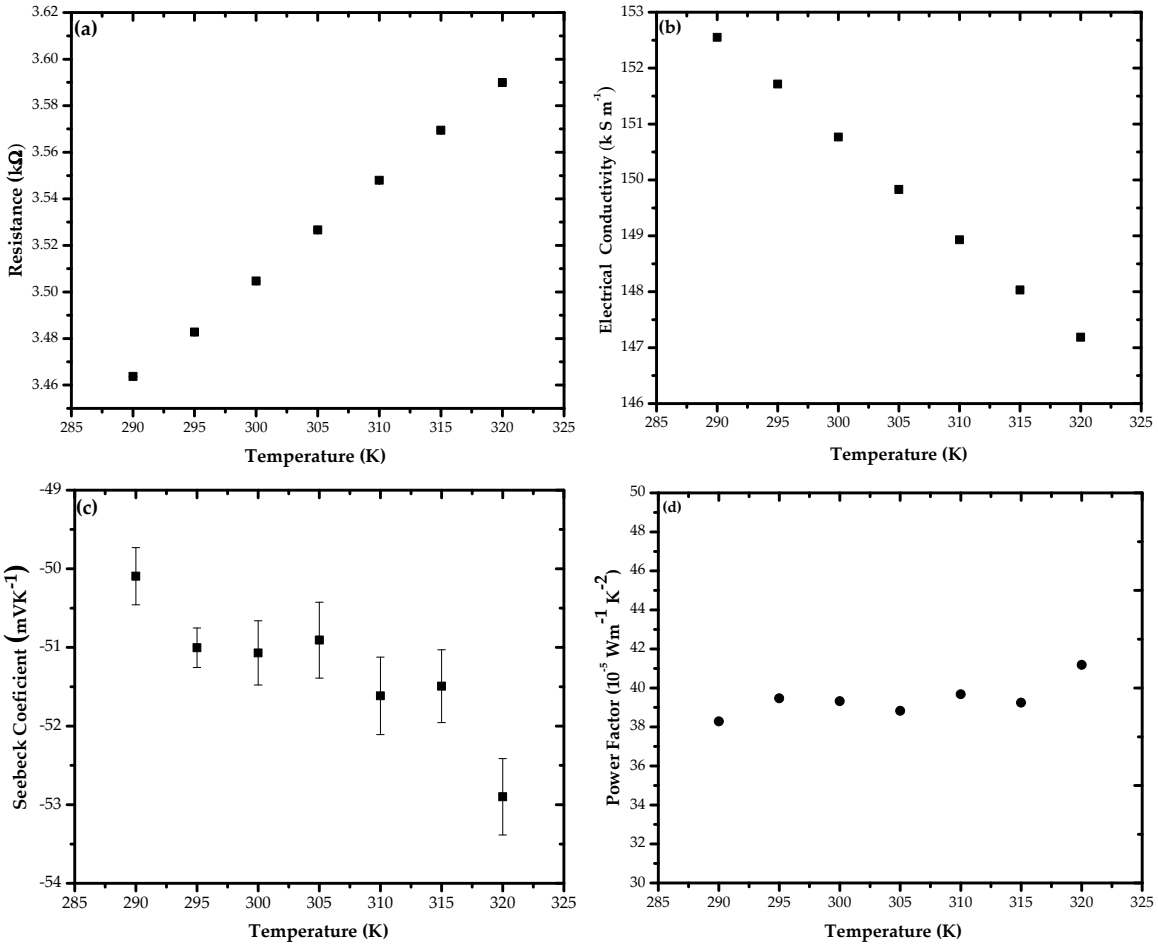

Figure 3. Temperature dependence regarding the (**a**) electrical resistance, (**b**) electrical conductivity, (**c**) TE power (S) and (**d**) power factor of the single-crystal Bi_2S_3 NW.

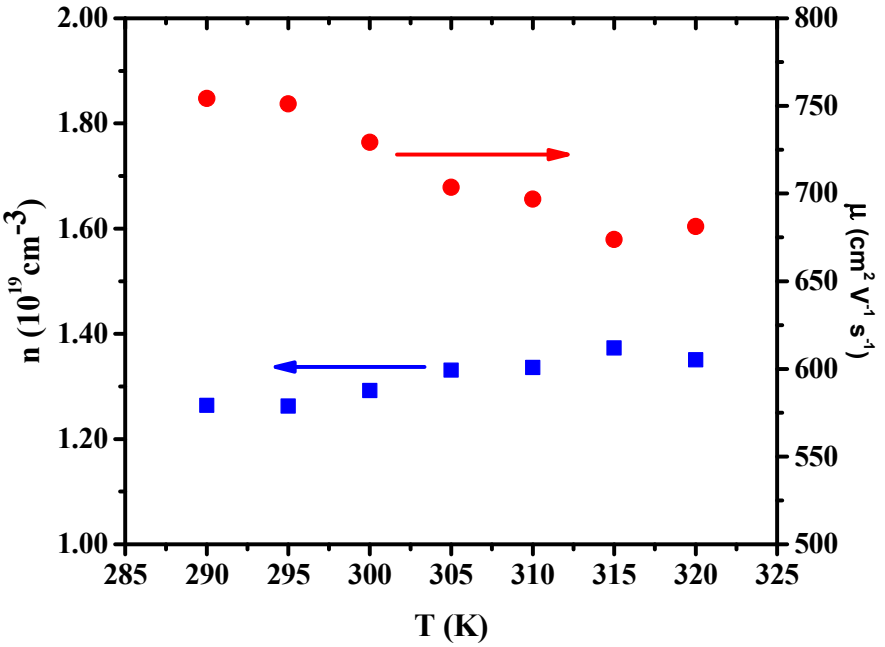

Figure 4. Temperature dependence of carrier concentration and carrier mobility for Bi_2Se_3 NW.

Figure 4 also depicts the calculated T dependences of carrier mobility μ for the Bi_2Se_3 NW. The μ value is obtained using the following equation:

$$\mu = \frac{1}{\rho n q} = \frac{\sigma}{nq} \tag{3}$$

Our calculated values of μ at 290–320 K were 754–681 cm^2 V^{-1} s^{-1} for the 200 nm NW; these values were much smaller than those of the Bi_2Se_3 bulk (approximately 920–1060 cm^2 V^{-1} s^{-1}) [41], but higher than those reported by Le et al. [60] for Bi_2Se_3 TFs (7.2 ± 0.2 to 98.4 ± 0.5 cm^2 V^{-1} s^{-1}). The μ values decreased as temperature increased because of the phonon concentration increase that caused increased scattering. Thus, lattice scattering reduced the carrier mobility at higher temperature. The mobility of a semiconductor depends on the impurity concentrations (including donor and acceptor concentrations), defect concentration, temperature, and electron and hole concentrations.

The primary factor involved in determining μ in the semiconductor is the scattering mechanism through the relation $\mu_j \propto T^{\alpha}$ [61]. Conduction carriers are scattered by acoustic phonons μ_l when $\alpha = -\frac{3}{2}$, whereas they are scattered by ionized impurities μ_i when $\alpha = \frac{3}{2}$. The μ values of the 200 nm Bi_2Se_3 NW continually decreased as the T increased, indicating that phonon scattering was dominant throughout the whole temperature range.

The thermal conductivity of Bi_2Se_3 NW was measured by the self-heating 3ω method in the temperature range of 290–320 K. The 3ω signal can be expressed as [62,63]:

$$V_{3\omega} = \frac{4I_0^3 LRR'}{\pi^4 \kappa S \sqrt{1 + (2\omega\gamma)^2}} \tag{4}$$

where I and ω are the amplitude and frequency of the alternating current applied on the nanowire, respectively; R and R' are the resistance and derivative of resistance at the corresponding temperature, respectively; κ is the thermal conductivity; S is the NW cross-section area; and γ is the characteristic thermal time constant. Figure 5a shows the current dependence of $V_{3\omega}$ at 300 K, demonstrating an I_0 dependence in an intermediate current range; one can see that $V_{3\omega}(I_0)$ followed the ${I_0}^3$ dependence well, in agreement with Equation (4). Figure 5b,c show the frequency dependencies of the amplitude and the

phase angle of $V_{3\omega}$ at 300 K, respectively, compared with the predicted functional forms (the solid lines). The fitting parameters for Figure 5a,b are shown in Tables S1 and S2, respectively.

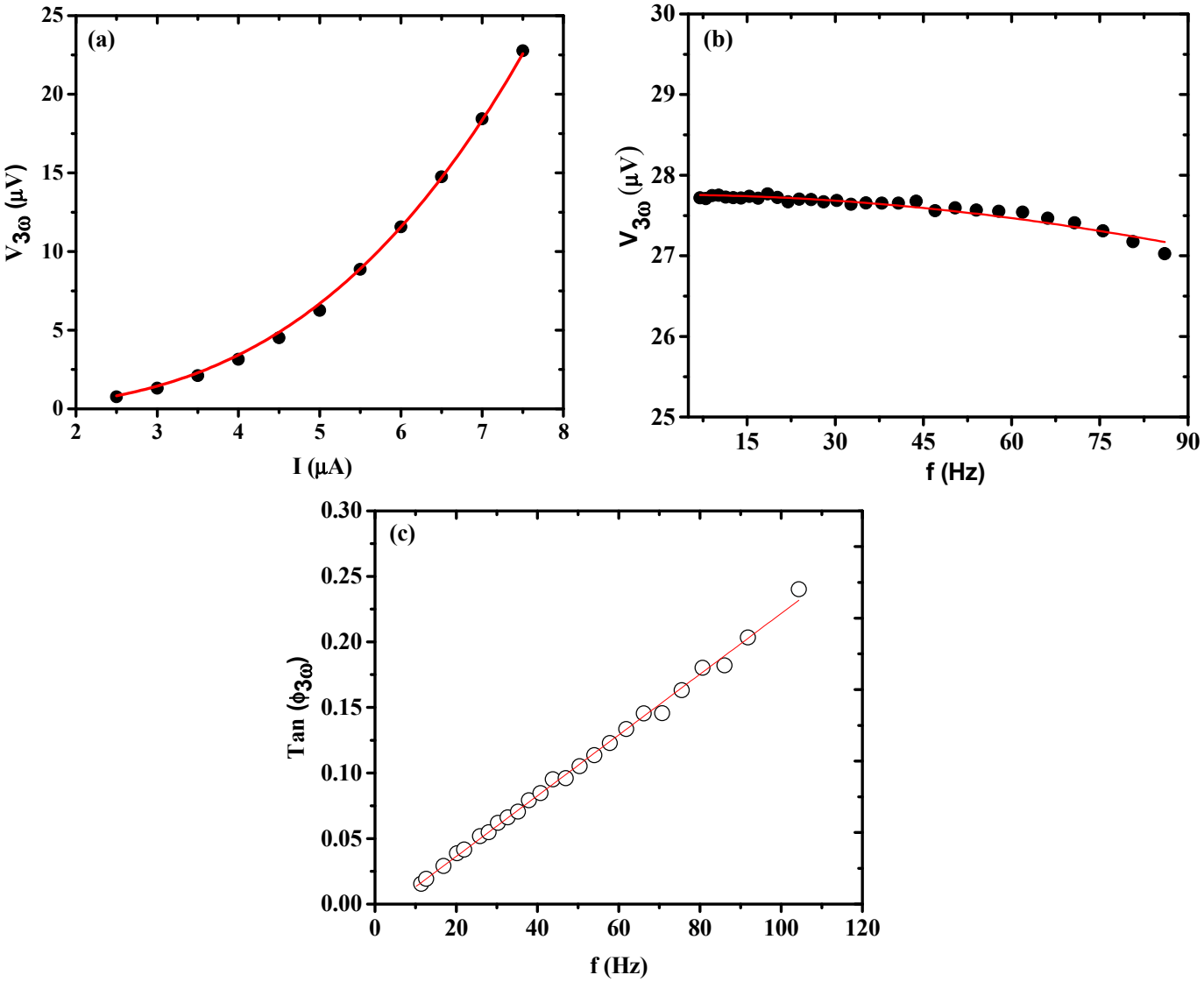

Figure 5. (**a**) The third harmonic voltage signal V3ω as function of the extraction current amplitude I_o. The solid line shows the cubic relationship of V3ω and I_o. (**b**) Frequency dependence of V3ω. The solid line is the predicted relation $V3\omega \propto 1/\sqrt{1+(2\omega\gamma)^2}$. (**c**) The frequency dependence of the phase angle of V3ω at 300 K of Bi_2Se_3 NW; d = 200 nm.

By fitting the data in Figure 5a to equation $V_{3\omega} = \frac{4I_0^3 LRR'}{\pi^4 \kappa S}$ ($\omega\gamma \rightarrow 0$), we obtained the thermal conductivity κ, and the thermal time constant γ was ~2 ms at 300 K, comparable to a simple theoretical calculation of κ based on the Callaway model for nanostructured Bi_2Se_3 made by Li et al. [64,65]. It is known that phonon-boundary scattering can suppress the thermal conductivity in nanowires [66,67]. However, the data on a Bi_2Se_3 NW with d = 200 nm from the experimental κ values (κ = 2.02 to 2.09 W m^{-1} K^{-1} at 290–320 K) as plotted in Figure 6a are in reasonable agreement with the Callaway model between the κ values of 300 nm (κ > 2 W m^{-1} K^{-1}) and 100 nm (κ < 2 W m^{-1} K^{-1}) [64]. The measured thermal conductivity, given by the κ value (κ is measured perpendicular to c plane) at T = 300 K of the NW (2.05 W m^{-1} K^{-1}) was ~33% lower than those for Bi_2Se_3 bulk single-crystal (2.96 W m^{-1} K^{-1} or 3.1 W m^{-1} K^{-1} in Table 1) [39,41].

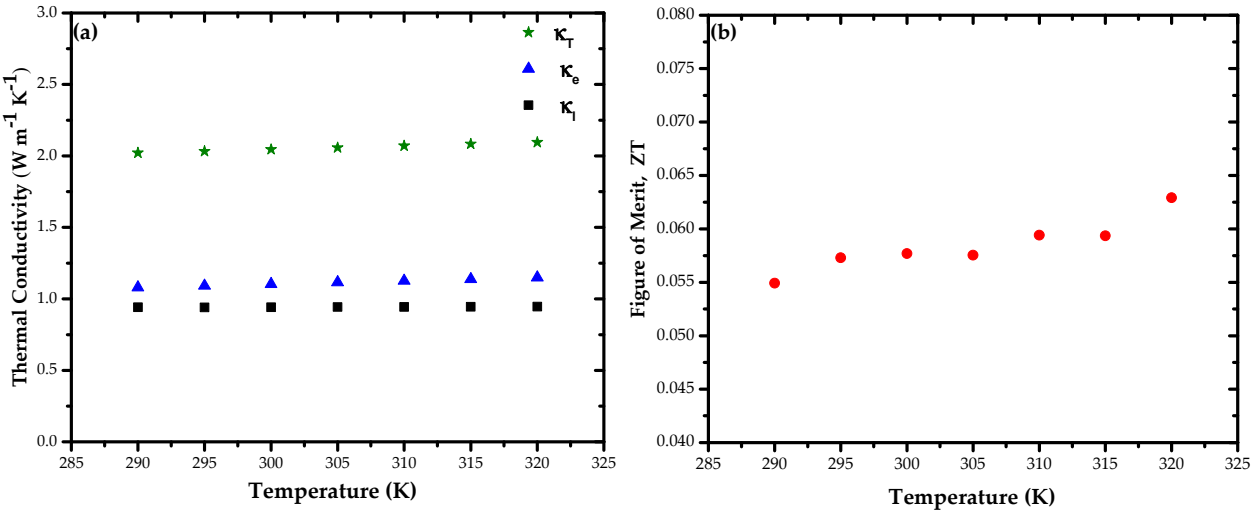

Figure 6. (**a**) Thermal conductivity κ, and (**b**) figure of merit *ZT* values of Bi_2Se_3 NW in the temperature range of 290 K to 320 K.

Table 1. The transport properties of Bi_2Se_3 nanowire and bulk at room temperature.

Sample *	S [μV K^{-1}]	Σ [S m^{-1}]	PF [10^{-5} W m^{-1}K^{-2}]	κ W m^{-1}K^{-1}	ZT	Ref.
Bi_2Se_3	−53	38678	10.70	0.78	0.04	[26]
Bi_2Se_3	−115	212	2.80	0.75	0.01	[28]
$Bi_2Se_{2.83}$	−60	25000	9	0.55	0.05	[29]
Bi_2Se_3 Nanowire SC (φ = 200 nm)	−51	150767	39.32	2.05	0.06	Our Work
Bi_2Se_3 Bulk SC	−62.10	259998	100	1.55	0.19	Our Work
Bi_2Se_3 Bulk SC	−190	47619	172	2.96	0.17	[39]
Bi_2Se_3 Bulk SC	−59	275500	95.90	3.1	0.09	[41]

* SC = single-crystalline.

The electronic thermal conductivity κ_e values of the Bi_2Se_3 NWs here were calculated according to the Wiedemann–Franz law:

$$\kappa_e = L\sigma T \quad (5)$$

where *L* is the Lorenz number (2.44×10^{-8} W Ω K^{-2}). When subtracting the κ_e values from the measured thermal conductivity, one obtains the phonon (or lattice) part of the thermal conductivity as $\kappa_l = \kappa\text{-}\kappa_e$. The temperature-dependent data for κ_l thus obtained are shown in Figure 6a. The obtained for κ_l and κ_e at 300 K for NWs were 29% and 37% lower than that of the Bi_2Se_3 bulk single-crystal (κ_l = 1.33 W m^{-1} K^{-1} and κ_e = 1.77 W m^{-1} K^{-1}) [41]. The thermal conductivity was dominated by the electronic contribution in the 290–320 K range, although Birkholz and Rosi both reported a value for κ_l of Bi_2Se_3 bulk of between 2.0 and 2.4 W m^{-1} K^{-1} [51]. It was shown that the large surface-to-volume ratio s/v of nanowires could enhance phonon surface scattering and decrease κ_l.

Additionally, for this nanowire, *ZT* calculated from the obtained *S*, σ, and κ was approximately 0.06 at 300 K (Figure 6b). However, the *ZT* values of this nanowire were still higher than those of Bi_2Se_3 bulk used to construct nanostructures at 290–320 K, as reported previously [26,28,29]. Table 1 shows a summary of the transport properties of single-crystalline Bi_2Se_3 NW, compared with those reported Bi_2Se_3 bulk at room temperature. Our *S*, *σ*, and *κ* results of Bi_2Se_3 NW *d* = 200 nm were in reasonable agreement with a theoretical study [19]. This agreement indicates the high-quality crystallinity of the Bi_2Se_3 NWs grown by the stress-induced method.

4. Conclusions

The stress-induced method was applied to grow single-crystalline Bi_2Se_3 nanowires (NWs) from a Bi_2Se_3 TF on a SiO_2/Si substrate, offering an alternative technique for Bi_2Se_3 NWs synthesis without a catalyst. This technique had not been previously applied to

Bi_2Se_3 alloys. In this work, at room temperature, the Bi_2Se_3 nanowire (NW) (d = 200 nm) exhibited a *PF* of approximately 39.32 × 10^{-5} $Wm^{-1}K^{-2}$, which was higher than that reported for Bi_2Se_3 bulk nanostructures; this discrepancy was mainly attributed to the electron-transport contribution of this NW. The measured thermal conductivity κ value of a NW was 2.05 W m^{-1} K^{-1}, which was 31−34% lower than those for a Bi_2Se_3 bulk single crystal [39,41] because of the electron-scattering contribution. The figure of merit *ZT* value of Bi_2Se_3 NW rose up to approximately 0.06 at room temperature, in agreement with a theoretical study of the thermoelectric properties on a topological insulator of Bi_2Se_3 NWs [19]. Our results indicated that NWs grown using the stress-induced method yield high-quality single crystals.

Supplementary Materials: The following are available online at https://www.mdpi.com/2079-4991/11/3/819/s1, Figure S1: (a) Image of Bi_2Se_3 single-crystalline grown by the Bridgman method. (b) The measured thermoelectric properties were −62.10 μ VK^{-1}, 259998 S m^{-1}, 1.55 W m^{-1} K^{-1}, and 0.19 for the Seebeck coefficient (S), electrical conductivity (σ), thermal conductivity (κ) and figure of merit *ZT*, respectively, at room temperature, as shown in Table 1, Table S1: The fitting parameters of the third harmonic voltage signal V3ω as function of the extraction current amplitude Io for Figure 5a, Table S2: The fitting parameters of frequency dependence of V3ω for Figure 5b.

Author Contributions: Conceptualization, D. and Y.-Y.C.; methodology, D., P.-C.W. and P.-C.L.; software, D. and P.-C.L.; validation, D. and Y.-Y.C.; formal analysis, D., P.-C.L. and Y.-Y.C.; investigation, D., P.-C.L. and Y.-Y.C.; resources, D., P.-C.W. and P.-C.L.; data curation, D., P.-C.L. and Y.-Y.C.; writing—original draft preparation, D.; writing—review and editing, D., P.-C.L. and Y.-Y.C.; visualization, D.; project administration, P.-C.L. and Y.-Y.C.; supervision, Y.-Y.C.; funding acquisition, D. and Y.-Y.C., All authors have read and agreed to the published version of the manuscript.

Funding: This study was funded by the National Science Council of Taiwan (grant NSC 100-2112-M-001-019-MY3), and the publishing fee was supported by the Research Center for Electronics and Telecommunications (P2ET), Indonesian Institute of Sciences (LIPI).

Data Availability Statement: The data presented in this study are available on request from the corresponding author.

Acknowledgments: The authors wish to thank the Core Facilities for Nanoscience and Nanotechnology at the Institute of Physics of the Academia Sinica in Taiwan for providing technical support.

Conflicts of Interest: The authors declare no conflict of interest.

References

1. Boukai, A.I.; Bunimovich, Y.; Tahir-Kheli, J.; Yu, J.K.; Goddard, W.A.; Heath, J.R. Silicon nanowires as efficient thermoelectric materials. *Nature* **2008**, *451*, 168–171. [CrossRef]
2. Bubnova, O.; Khan, Z.U.; Malti, A.; Braun, S.; Fahlman, M.; Berggren, M.; Crispin, X. Optimization of the thermoelectric figure of merit in the conducting polymer poly(3,4-ethylenedioxythiophene). *Nat. Mater.* **2011**, *10*, 429–433. [CrossRef]
3. Hochbaum, A.I.; Chen, R.; Delgado, R.D.; Liang, W.; Garnett, E.C.; Najarian, M.; Majumdar, A.; Yang, P. Enhanced thermoelectric performance of rough silicon nanowires. *Nature* **2008**, *451*, 163–167. [CrossRef]
4. Minnich, A.J.; Dresselhaus, M.S.; Ren, Z.F.; Chen, G. Bulk nanostructured thermoelectric materials: Current research and future prospects. *Energy Environ. Sci.* **2009**, *2*, 466–479. [CrossRef]
5. Zhao, H.; Pokheral, M.; Zhu, G.; Chen, S.; Lukas, K.; Jie, Q.; Opeil, C.; Chen, G.; Ren, Z. Dramatic thermal conductivity reduction by nanostructures for large increase in thermoelectric figure-of-merit of FeSb2. *Appl. Phys. Lett.* **2011**, *99*, 2012–2015. [CrossRef]
6. Snyder, G.J.; Toberer, E.S. Complex thermoelectric materials. *Mater. Sustain. Energy Collect. Peer Rev. Res. Rev. Artic. Nat. Publ. Group* **2010**, *7*, 101–110.
7. Tritt, T.M.; Subramanian, M.A. Thermoelectric Materials, Phenomena and Applications: A Bird's Eye View. *MRS bulletin* **2006**, *31*, 188–198. [CrossRef]
8. Disalvo, F.J. Thermoelectric cooling and power generation. *Science* **1999**, *285*, 703–706. [CrossRef]
9. Tritt, T.M. Thermoelectric materials:Holey and Unholey Semiconductors. *Science* **1999**, *283*, 804–805. [CrossRef]
10. Rowe, D.M. *CRC Handbook of Thermoelectrics*; CRC Press: Danvers, MA, USA, 1995; ISBN 0849301467.
11. Dresselhaus, M.S.; Chen, G.; Tang, M.Y.; Yang, R.; Lee, H.; Wang, D.; Ren, Z.; Fleurial, J.P.; Gogna, P. New directions for low-dimensional thermoelectric materials. *Adv. Mater.* **2007**, *19*, 1043–1053. [CrossRef]
12. Mahan, G.D.; Sofo, J.O. The best thermoelectric. *Proc. Natl. Acad. Sci. USA* **1996**, *93*, 7436–7439. [CrossRef]

13. Lin, Y.M.; Sun, X.; Dresselhaus, M. Theoretical investigation of thermoelectric transport properties of cylindrical Bi nanowires. *Phys. Rev. B* **2000**, *62*, 4610–4623. [CrossRef]
14. Hicks, L.; Dresselhaus, M.S. Effect of quantum-well structures on the thermoelectric figure of merit. *Phys. Rev. B* **1993**, *47*, 12727. [CrossRef]
15. Boukai, A.; Xu, K.; Heath, J.R. Size-dependent transport and thermoelectric properties of individual polycrystalline bismuth nanowires. *Adv. Mater.* **2006**, *18*, 864–869. [CrossRef]
16. Slack, G. New Materials and Performance Limits for Thermoelectric Cooling. In *CRC Handbok Thermoelectrics*; CRC Press: Danvers, MA, USA, 1995.
17. Mishra, S.K.; Satpathy, S.; Jepsen, O. Electronic structure and thermoelectric properties of bismuth telluride and bismuth selenide. *J. Phys. Condens. Matter* **1997**, *9*, 461–470. [CrossRef]
18. Al Bayaz, A.; Giani, A.; Foucaran, A.; Pascal-Delannoy, F.; Boyer, A. Electrical and thermoelectrical properties of Bi2Se3 grown by metal organic chemical vapour deposition technique. *Thin Solid Films* **2003**, *441*, 1–5. [CrossRef]
19. Gooth, J.; Gluschke, J.G.; Zierold, R.; Leijnse, M.; Linke, H.; Nielsch, K. Thermoelectric performance of classical topological insulator nanowires. *Semicond. Sci. Technol.* **2015**, *30*, 015015. [CrossRef]
20. Watanabe, K.; Sato, N.; Miyaoka, S. New optical recording material for video disc system. *J. Appl. Phys.* **1983**, *54*, 1256–1260. [CrossRef]
21. Waters, J.; Crouch, D.; Raftery, J.; O'Brien, P. Deposition of bismuth chalcogenide thin films using novel single-source precursors by metal-organic chemical vapor deposition. *Chem. Mater.* **2004**, *16*, 3289–3298. [CrossRef]
22. Venkatasubramanian, R.; Siivola, E.; Colpitts, T.; O'Quinn, B. Thin-film thermoelectric devices with high room-temperature figures of merit. *Nature* **2001**, *413*, 597–602. [CrossRef] [PubMed]
23. Xu, H.; Chen, G.; Jin, R.; Pei, J.; Wang, Y.; Chen, D. Hierarchical Bi2Se3 microrods: Microwave-assisted synthesis, growth mechanism and their related properties. *Cryst. Eng. Comm.* **2013**, *15*, 1618–1625. [CrossRef]
24. Xu, H.; Chen, G.; Jin, R.; Chen, D.; Wang, Y.; Pei, J.; Zhang, Y.; Yan, C.; Qiu, Z. Microwave-assisted synthesis of Bi2Se3 ultrathin nanosheets and its electrical conductivities. *Cryst. Eng. Comm.* **2014**, *16*, 3965–3970. [CrossRef]
25. Lin, Y.F.; Chang, H.W.; Lu, S.Y.; Liu, C.W. Preparation, characterization, and electrophysical properties of nanostructured BiPO4 and Bi2Se3 derived from a structurally characterized, single-source precursor $Bi[Se_2P(OiPr)_2]_3$. *J. Phys. Chem. C* **2007**, *111*, 18538–18544. [CrossRef]
26. Bai, T.; Li, C.; Liang, D.; Li, F.; Jin, D.; Shi, Z.; Feng, S. Synthesis of various metal selenide nanostructures using the novel selenium precursor 1,5-bis(3-methylimidazole-2-selone)pentane. *Cryst. Eng. Comm.* **2013**, *15*, 6483–6490. [CrossRef]
27. Manjare, S.T.; Yadav, S.; Singh, H.B.; Butcher, R.J. Redox reaction between main-group elements (Te, Sn, Bi) and N-Heterocyclic-carbene-derived selenium halides: A facile method for the preparation of monomeric halides. *Eur. J. Inorg. Chem.* **2013**, *2013*, 5344–5357. [CrossRef]
28. Kadel, K.; Kumari, L.; Li, W.Z.; Huang, J.Y.; Provencio, P.P. Synthesis and thermoelectric properties of Bi_2Se_3 nanostructures. *Nanoscale Res. Lett.* **2011**, *6*, 57. [CrossRef] [PubMed]
29. Min, Y.; Roh, J.W.; Yang, H.; Park, M.; Kim, S.I.; Hwang, S.; Lee, S.M.; Lee, K.H.; Jeong, U. Surfactant-free scalable synthesis of Bi_2Te_3 and Bi_2Se_3 nanoflakes and enhanced thermoelectric properties of their nanocomposites. *Adv. Mater.* **2013**, *25*, 1425–1429. [CrossRef] [PubMed]
30. Sun, Z.; Liufu, S.; Chen, L. Synthesis and characterization of nanostructured bismuth selenide thin films. *Dalt. Trans.* **2010**, *39*, 10883–10887. [CrossRef] [PubMed]
31. Giani, A.; Al Bayaz, A.; Foucaran, A.; Pascal-Delannoy, F.; Boyer, A. Elaboration of Bi_2Se_3 by metalorganic chemical vapour deposition. *J. Cryst. Growth* **2002**, *236*, 217–220. [CrossRef]
32. Alegria, L.D.; Schroer, M.D.; Chatterjee, A.; Poirier, G.R.; Pretko, M.; Patel, S.K.; Petta, J.R. Structural and electrical characterization of Bi 2Se 3 nanostructures grown by metal-organic chemical vapor deposition. *Nano Lett.* **2012**, *12*, 4711–4714. [CrossRef]
33. Sun, Y.; Cheng, H.; Gao, S.; Liu, Q.; Sun, Z.; Xiao, C.; Wu, C.; Wei, S.; Xie, Y. Atomically thick bismuth selenide freestanding single layers achieving enhanced thermoelectric energy harvesting. *J. Am. Chem. Soc.* **2012**, *134*, 20294–20297. [CrossRef]
34. Checkelsky, J.G.; Hor, Y.S.; Cava, R.J.; Ong, N.P. Bulk band gap and surface state conduction observed in voltage-tuned crystals of the topological insulator Bi_2Se_3. *Phys. Rev. Lett.* **2011**, *106*, 4–7. [CrossRef] [PubMed]
35. Hong, S.S.; Kundhikanjana, W.; Cha, J.J.; Lai, K.; Kong, D.; Meister, S.; Kelly, M.A.; Shen, Z.X.; Cui, Y. Ultrathin topological insulator Bi_2Se_3 nanoribbons exfoliated by atomic force microscopy. *Nano Lett.* **2010**, *10*, 3118–3122. [CrossRef]
36. Janíček, P.; Drašar, Č.; Beneš, L.; Lošťák, P. Thermoelectric properties of Tl-doped Bi_2Se_3 single crystals. *Cryst. Res. Technol.* **2009**, *44*, 505–510. [CrossRef]
37. King, M.D.; Blanton, T.N.; Misture, S.T.; Korter, T.M. Prediction of the unknown crystal structure of creatine using fully quantum mechanical methods. *Cryst. Growth Des.* **2011**, *11*, 5733–5740. [CrossRef]
38. Kašparová, J.; Drašar, Č.; Krejčová, A.; Beneš, L.; Lošťák, P.; Chen, W.; Zhou, Z.; Uher, C. n-type to p-type crossover in quaternary Bi xSb yPb zSe 3 single crystals. *J. Appl. Phys.* **2005**, *97*, 103720. [CrossRef]
39. Hor, Y.S.; Richardella, A.; Roushan, P.; Xia, Y.; Checkelsky, J.G.; Yazdani, A.; Hasan, M.Z.; Ong, N.P.; Cava, R.J. P-type Bi_2Se_3 for topological insulator and low-temperature thermoelectric applications. *Phys. Rev. B* **2009**, *79*, 195208. [CrossRef]
40. Qiu, X.; Austin, L.N.; Muscarella, P.A.; Dyck, J.S.; Burda, C. Nanostructured Bi_2Se_3 films and their thermoelectric transport properties. *Angew. Chem. Int. Ed.* **2006**, *45*, 5656–5659. [CrossRef]

41. Navrátil, J.; Horák, J.; Plecháček, T.; Kamba, S.; Lošťák, P.; Dyck, J.S.; Chen, W.; Uher, C. Conduction band splitting and transport properties of Bi_2Se_3. *J. Solid State Chem.* **2004**, *177*, 1704–1712. [CrossRef]
42. Dedi; Lee, P.C.; Chien, C.H.; Dong, G.P.; Huang, W.C.; Chen, C.L.; Tseng, C.M.; Harutyunyan, S.R.; Lee, C.H.; Chen, Y.Y. Stress-induced growth of single-crystalline lead telluride nanowires and their thermoelectric transport properties. *Appl. Phys. Lett.* **2013**, *103*, 1–6. [CrossRef]
43. Dedi; Chien, C.H.; Hsiung, T.C.; Chen, Y.C.; Huang, Y.C.; Lee, P.C.; Lee, C.H.; Chen, Y.Y. Structural, electronic transport and magnetoresistance of a 142nm lead telluride nanowire synthesized using stress-induced growth. *AIP Adv.* **2014**, *4*, 1–7. [CrossRef]
44. Cheng, Y.T.; Weiner, A.M.; Wong, C.A.; Balogh, M.P.; Lukitsch, M.J. Stress-induced growth of bismuth nanowires. *Appl. Phys. Lett.* **2002**, *81*, 3248–3250. [CrossRef]
45. Shim, W.; Ham, J.; Lee, K.; Jeung, W.Y.; Johnson, M.; Lee, W. On-film formation of Bi nanowires with extraordinary electron mobility. *Nano Lett.* **2009**, *9*, 18–22. [CrossRef]
46. Chen, X.; Zhou, H.D.; Kiswandhi, A.; Miotkowski, I.; Chen, Y.P.; Sharma, P.A.; Lima Sharma, A.L.; Hekmaty, M.A.; Smirnov, D.; Jiang, Z. Thermal expansion coefficients of Bi_2Se_3 and Sb_2Te_3 crystals from 10 K to 270 K. *Appl. Phys. Lett.* **2011**, *99*, 12–15. [CrossRef]
47. Kong, D.; Randel, J.C.; Peng, H.; Cha, J.J.; Meister, S.; Lai, K.; Chen, Y.; Shen, Z.X.; Manoharan, H.C.; Cui, Y. Topological insulator nanowires and nanoribbons. *Nano Lett.* **2010**, *10*, 329–333. [CrossRef] [PubMed]
48. Wang, D.; Sheriff, B.A.; Heath, J.R. Complementary symmetry silicon nanowire logic: Power-efficient inverters with gain. *Small* **2006**, *2*, 1153–1158. [CrossRef] [PubMed]
49. Partin, D.L. Growth and characterization of epitaxial bismuth films. *J. Vac. Sci. Technol. B Microelectron. Nanom. Struct.* **1989**, *7*, 348. [CrossRef]
50. De Kuijper, A.H.; Bisschop, J. Temperature dependence of concentrations and mobilities in thin bismuth films. *Thin Solid Films* **1983**, *110*, 99–106. [CrossRef]
51. Nolas, G.S.; Sharp, J.; Goldsmid, J. *Thermoelectrics: Basic Principles and New Materials Developments*; Springer-Verlag: Berlin/Heidelberg, Germany, 2013; Volume 45, ISBN 9781461257080.
52. Greenaway, D.L.; Harbeke, G. Band structure of bismuth telluride, bismuth selenide and their respective alloys. *J. Phys. Chem. Solids* **1965**, *26*, 1585–1604. [CrossRef]
53. Dedi; Idayanti, N.; Lee, P.-C.; Lee, C.-H.; Chen, Y.-Y. Thermoelectric power of single crystalline lead telluride nanowire. *J. Phys. Conf. Ser.* **2016**, *776*, 012046. [CrossRef]
54. Kim, D.; Syers, P.; Butch, N.P.; Paglione, J.; Fuhrer, M.S. Ambipolar surface state thermoelectric power of topological insulator Bi2Se3. *Nano Lett.* **2014**, *14*, 1701–1706. [CrossRef] [PubMed]
55. Cutler, M.; Mott, N.F. Observation of anderson localization in an electron gas. *Phys. Rev.* **1969**, *181*, 1336–1340. [CrossRef]
56. Wang, Z.; Lin, T.; Wei, P.; Liu, X.; Dumas, R.; Liu, K.; Shi, J. Tuning carrier type and density in Bi_2Se_3 by Ca-doping. *Appl. Phys. Lett.* **2010**, *97*, 2012–2015. [CrossRef]
57. Horák, J.; Navrátil, J.; Starý, Z. Lattice point defects and free-carrier concentration in Bi_2+xTe_3 and Bi_2+xSe_3 crystals. *J. Phys. Chem. Solids* **1992**, *53*, 1067–1072. [CrossRef]
58. Lee, C.H.; Yi, G.C.; Zuev, Y.M.; Kim, P. Thermoelectric power measurements of wide band gap semiconducting nanowires. *Appl. Phys. Lett.* **2009**, *94*, 1–4. [CrossRef]
59. Wolpert, D.; Ampadu, P. *Managing Temperature Effects in Nanoscale Adaptive Systems*; Hardcover; Springer-Verlag: New York, NY, USA, 2012; Volume XXII, pp. 1–174, ISBN 978-1-4614-0747-8.
60. Le, P.H.; Liao, C.N.; Luo, C.W.; Lin, J.Y.; Leu, J. Thermoelectric properties of bismuth-selenide films with controlled morphology and texture grown using pulsed laser deposition. *Appl. Surf. Sci.* **2013**, *285*, 657–663. [CrossRef]
61. Sze, S.M.; Ng, K.K. *Physics of Semiconductor Devices*, 3th ed.; Wiley: Danvers, MA, USA, 2007; ISBN 978-0-471-14323-9.
62. Lu, L.; Yi, W.; Zhang, D.L. 3 Ω method for specific heat and thermal conductivity measurements. *Rev. Sci. Instrum.* **2001**, *72*, 2996–3003. [CrossRef]
63. Dedi; Primadona, I.; Lee, P.C.; Chien, C.H.; Chen, Y.Y. Structural and Thermoelectric Properties Characterization of Individual Single-Crystalline Nanowire. In *Impact of Thermal Conductivity on Energy Technologies*; Shahzad, A., Ed.; IntechOpen: London, UK, 2018; pp. 149–166, ISBN 978-1-78923-673-6.
64. Li, G.; Liang, D.; Qiu, R.L.J.; Gao, X.P.A. Thermal conductivity measurement of individual Bi_2Se_3 nano-ribbon by self-heating three-ω method. *Appl. Phys. Lett.* **2013**, *102*, 043104. [CrossRef]
65. Callaway, J. Model for lattice thermal conductivity at low temperatures. *Phys. Rev.* **1959**, *113*, 1046–1051. [CrossRef]
66. Zhou, J.; Jin, C.; Seol, J.H.; Li, X.; Shi, L. Thermoelectric properties of individual electrodeposited bismuth telluride nanowires. *Appl. Phys. Lett.* **2005**, *87*, 133109. [CrossRef]
67. Li, D.; Wu, Y.; Kim, P.; Shi, L.; Yang, P.; Majumdar, A. Thermal conductivity of individual silicon nanowires. *Appl. Phys. Lett.* **2003**, *83*, 2934–2936. [CrossRef]